

Optimizing Probabilistic Constellation Shaping for Amplifier-Less Coherent Optical Links

Beatriz M. Oliveira , Abel Lorences-Riesgo , Fernando P. Guiomar , Maria C. R. Medeiros ,
and Paulo P. Monteiro 

Abstract—Coherent optical systems for short-reach links have seen a boost in their popularity with the standardization of 400ZR. These systems need to be cost and power-efficient, while coping with the ever increase in traffic demand. The use of probabilistic constellation shaping (PCS) can help meet these demands, since it reduces the gap to the channel capacity. However, studies concerning PCS typically include optical amplification; therefore, its gain in amplifier-less systems has been somewhat uncertain. In this work, we focus on an amplifier-less coherent optical link employing PCS, reducing both power consumption and system complexity due to the removal of the amplifier. We employ PCS for different modulation orders and bit rates, while optimizing several key parameters such as the FEC coding overhead, modulation depth and clipping. With this comprehensive study, we demonstrate by system simulation and experimental validation that PCS is beneficial even for amplifier-less systems, since it introduces residual gains while allowing higher flexibility in defining the net bit rate in a system with fixed baud rate.

Index Terms—Coherent optical systems, probabilistic constellation shaping, amplifier-less.

I. INTRODUCTION

AFTER becoming a dominant technology in long-haul terrestrial and subsea fiber links, coherent optical systems are now progressively entering the short-reach sector [1]. As the continuous rise in traffic demand imposes higher data rates, coherent transceivers provide a future-proof alternative to the traditional use of intensity modulation and direct detection (IM-DD), allowing for an increase in sensitivity and spectral efficiency, while also circumventing the bit rate limitation imposed by chromatic dispersion in IM-DD systems [2]. This led to the recent standardization of coherent optical interfaces for short-reach 400G systems [3], with numerous prospective

applications, including passive optical networks [4], inter data-center [5] and fronthaul links [6].

Despite the tremendous potential of coherent optical interfaces, their commercial success in the competitive short-reach market still depends on significant further improvements in terms of power consumption and cost [6]–[8]. Several recent studies have been addressing this challenge through different approaches, namely by using enhanced modulation techniques [9]–[12] in order to reduce the cost per bit, and by simplifying the transmitter [13] and/or receiver [14]–[16] hardware. Aside from these necessary improvements at the transceiver side, link-level optimization can also contribute to significantly reduce the overall cost of the system. In this sense, avoiding optical amplification becomes a key requirement to achieve both power and cost-effective systems, while still covering transmission distances compatible with short-reach applications. Furthermore, by keeping a low optical transmitted power, complex optical safety procedures are avoided during the operation and maintenance of deployed optical networks.

Probabilistic constellation shaping (PCS) is a technique that aims to reduce the modulation gap to the Shannon capacity limit, achieving a maximum theoretical shaping gain of 1.53 dB for additive white Gaussian noise (AWGN) channels [10], which can be a crucial aid in achieving the power and cost requirements for amplifier-less coherent systems. Despite its recent adoption in optical communications, PCS is already playing an important role in the literature, with a panoply of applications, including access networks [17], free-space optical links [18] and underwater visible light communications [19]. PCS is already being deployed in 800G application-specific integrated circuits (ASIC) [20], and compact form-factor pluggable (CFP) transceivers [21], enabling its use together with coherent communications in embedded cost-effective and low power systems. These studies take advantage of the PCS theoretical gain, as well as the fine granularity it allows in defining the net bit rate. As shown in [18], this can be of key importance to provide adaptability to the system's current signal-to-noise ratio (SNR). However, PCS still requires comprehensive studies for amplifier-less applications, where the power constraint imposed on the system enhances the impact of the modulation loss (i.e., the power loss caused by the modulation process), which may compromise the achievable shaping gain. Recently, a comparison between PCS and uniform constellations has revealed that PCS may not be able to provide any shaping gain in systems without a booster at the transmitter side [11]. This

This work was partially supported by the European Regional Development Fund (FEDER), through the Regional Operational Programme of Centre (CENTRO 2020) of the Portugal 2020 framework, through project ORCIP (CENTRO-01-0145-FEDER-022141), SOCA (CENTRO-01-0145-FEDER-000010), RETIOT (POCI-01-0145-FEDER-016432) and LANDMARK (POCI-01-0145-FEDER-031527), and by FCT/MCTES through project FreeComm-B5G (UIDB/EEA/50008/2020). Beatriz M. Oliveira acknowledges a PhD grant from FCT (SFRH/BD/143498/2019). Fernando P. Guiomar acknowledges a fellowship from “la Caixa” Foundation (ID 100010434). The fellowship code is LCF/BQ/PR20/11770015.

Beatriz M. Oliveira, Fernando P. Guiomar and Paulo P. Monteiro are with Instituto de Telecomunicações, University of Aveiro, 3810-193, Aveiro, Portugal (e-mail: beatriz.m.oliveira@ua.pt)

A. Lorences-Riesgo was with Instituto de Telecomunicações, 3810-193, Aveiro. He is now with Huawei Technologies France, 92100 Boulogne-Billancourt, France (abel.lorences.riesgo@huawei.com)

Maria C. R. Medeiros is with Instituto de Telecomunicações, Universidade de Coimbra, 3030-290, Coimbra, Portugal (email: cmedeiros@deec.uc.pt)

Manuscript received November 05, 2020; revised January 11, 2021.

result stems from the fact that PCS can increase the peak-to-average power ratio (PAPR) of the transmitted signal, thereby increasing the modulation loss, which is not compensated due to the absence of a booster amplifier. However, and as we have experimentally shown in [22], this loss can be minimized through the application of digital clipping together with the optimization of the amount of shaping and coding imposed on the transmitted signal. Therefore, it remains of utmost importance to clarify the actual role that PCS may play in next-generation coherent interfaces for amplifier-less short-reach applications.

In this work, we develop a comprehensive study on optimization of PCS modulation for amplifier-less single-span coherent systems, as an extension to the preliminary results presented in [22]. We study the impact of constellation order and shaping parameter, together with the optimization of digital clipping and modulation depth of the IQ modulator, providing a deeper understanding of the system and the potential gain of PCS. Thereby, we aim at delivering an extended answer to the previously debatable gain of PCS in amplifier-less systems.

The structure of this paper is as follows. After this introduction, section II presents a theoretical background, including definitions of the key parameters that will be optimized, such as the modulation depth, forward error correction (FEC) and probabilistic amplitude shaping (PAS) rate, and clipping of the transmitted signal. Section III shows simulation results for systems with and without optical amplification, evidencing the importance of optimizing the system's parameters. Section IV is composed of the experimental validation of section III. Section V concludes the paper.

II. THEORETICAL BACKGROUND

In this section, we briefly review a set of fundamental concepts regarding modulation, coding and shaping, whose precise definition is required to provide proper context to the numerical and experimental scenarios that will be introduced in sections III and IV.

A. IQ Modulator

The typical structure of an in-phase and quadrature modulator (IQM) is shown in Fig. 1. Considering an ideal implementation of the nested Mach-Zehnder modulator (MZM) architecture of Fig. 1, the IQM transfer function can be written as [23]

$$\frac{E_{\text{out}}}{E_{\text{in}}} = \frac{1}{2} \left[\sin\left(\frac{\pi}{2} M_D I_k\right) + \exp\left(j\frac{\pi}{2}\right) \sin\left(\frac{\pi}{2} M_D Q_k\right) \right], \quad (1)$$

where I_k and Q_k represent the baseband in-phase and quadrature signals for the k^{th} symbol, normalized to the range of $[-1, 1]$ and M_D represents the IQM modulation depth, defined as

$$M_D = \frac{V_{pp}}{2V_\pi}, \quad (2)$$

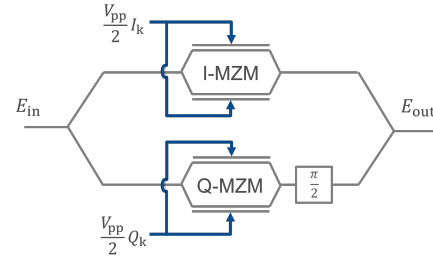


Fig. 1. Simplified architecture of a single-polarization in-phase and quadrature modulator (IQM).

where V_{pp} is the peak-to-peak amplitude of the electrical signals driving the MZMs¹ and V_π defines the switching voltage.

From expression (1), the optical power transfer of the IQM can then be obtained as

$$\begin{aligned} \frac{P_{\text{out}}}{P_{\text{in}}} &= E \left[\left| \frac{E_{\text{out}}}{E_{\text{in}}} \right|^2 \right] \\ &= \frac{1}{4} E \left[\sin^2\left(\frac{\pi}{2} M_D I_k\right) \right] + \frac{1}{4} E \left[\sin^2\left(\frac{\pi}{2} M_D Q_k\right) \right], \quad (3) \end{aligned}$$

where $E[\cdot]$ represents the expectation operator.

Assuming a square QAM constellation with i.i.d. symbols, then (3) can be reduced to

$$\frac{P_{\text{out}}}{P_{\text{in}}} = \frac{1}{2} E \left[\sin^2\left(\frac{\pi}{2} M_D I_k\right) \right]. \quad (4)$$

Finally, by defining the normalized in-phase component of the M -QAM signal, I_k , as

$$I_k = \frac{-\sqrt{M} + 2k - 1}{\sqrt{M} - 1}, \quad (5)$$

the power transfer of the IQM can be analytically derived as

$$\frac{P_{\text{out}}}{P_{\text{in}}} = \frac{1}{2\sqrt{M}} \sum_{k=1}^{\sqrt{M}} \sin^2 \left(-\frac{\pi}{2} \frac{\sqrt{M} - 2k + 1}{\sqrt{M} - 1} M_D \right), \quad (6)$$

which, after some algebraic manipulation, yields

$$\frac{P_{\text{out}}}{P_{\text{in}}} = \frac{1}{4} \left(1 - \frac{1}{\sqrt{M}} \frac{\sin\left(\frac{\pi M_D \sqrt{M}}{\sqrt{M} - 1}\right)}{\sin\left(\frac{\pi M_D}{\sqrt{M} - 1}\right)} \right). \quad (7)$$

Note that expression (7) already includes the contribution of the digital modulation-induced loss incurred by the use of a given M -QAM constellation. Furthermore, we have assumed that a rectangular pulse is fed to the IQM in order to define its power transfer function, and consider a close-to-ideal IQM model, taking only in consideration the nonlinearity caused by its sinusoidal transfer function. In addition, to simplify the equation we restrict this definition to $M = 2^n$.

Besides the dependence of the IQM power transfer on the modulation depth, it is also important to take into account the

¹For simplicity, it is assumed that the in-phase and quadrature arms of the IQM are fed by I and Q signals with the same peak-to-peak voltage.

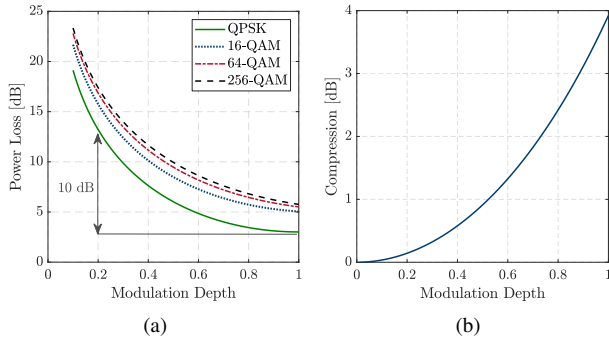


Fig. 2. a) Theoretical power loss and b) signal compression induced by the modulation depth of the IQM, M_D , for different M -QAM constellations.

nonlinear compression that comes along with the increase of M_D , which can be described by

$$C_{IQM} = -20 \log_{10} \left(\frac{\sin \left(\frac{\pi}{2} M_D \right)}{\frac{\pi}{2} M_D} \right). \quad (8)$$

Figure 2a shows the power loss stemming from expression (7), defined as $10 \log_{10} (P_{in}/P_{out})$, for different modulation depths and different constellation sizes. Notably, the power loss, in dB, shows a logarithmic dependence for low values of M_D , denoting a strong dependence of the IQM output power on the modulation depth. For instance, by increasing M_D from 0.1 to 0.2, the power loss of the IQM is reduced by approximately 6 dB, while keeping the IQM operating within a quasi-linear regime (see Fig. 2b, which shows the IQM compression as a function of M_D). This dependence then starts to become less pronounced as M_D increases towards unity. Nevertheless, it is interesting to note that the IQM power loss can be further reduced by about 10 dB when increasing M_D from 0.2 to 1, at the cost of operating the IQM in the nonlinear regime, with up to ~ 4 dB of signal compression.

Note that, for simplicity, the derivation of expression (7) has been presented for the case of a single-polarization IQM. Nevertheless, the same results are applicable to the case of a dual-polarization (DP) IQM. It is also worth referring that the use of pulse shaping filters and/or oversampling at the DAC might as well modify the PAPR of the transmitted signal and thereby influence the overall power loss incurred by the IQM. Nevertheless, the general trend of power loss dependence on M_D is expected to remain unchanged.

B. Peak-to-Average Power Ratio and Clipping

In practical systems with limited bit resolution in the digital-to-analog converter (DAC), the peak-to-average power ratio (PAPR) of the transmitted signal plays an important role. High PAPR imposes that a large portion of the signal, which is at low amplitude, suffers from enhanced quantization noise. Additionally, the average output power from the DAC is also reduced by the increase of PAPR. This behavior is aggravated with high modulation orders, especially when associated with PCS, which inherently increases the PAPR of the transmitted signal by reducing the probability of the outer QAM symbols. For this reason, it can be helpful to clip the

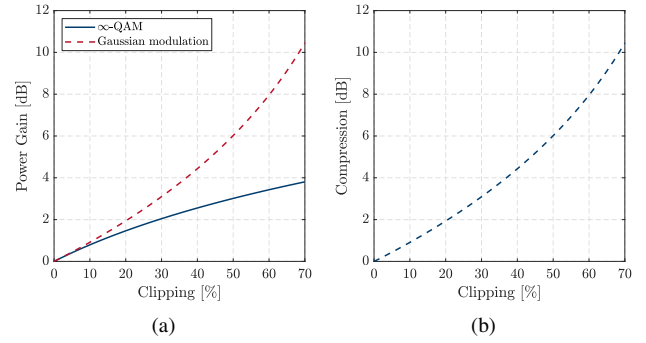


Fig. 3. a) Impact of clipping on amplification of the digital signal fed to the optical modulator. Two extreme scenarios are considered: a QAM signal with an infinite number of levels (∞ -QAM) and a Gaussian modulated signal. b) Signal compression induced by the applied clipping.

signal before transmission, thereby inherently decreasing the PAPR, which leads to lower quantization noise and higher transmitted average power. This effect can be even more beneficial for amplifier-less systems, effectively resulting in a process of *digital amplification* of the transmitted signal. However, excessive clipping can also decrease the performance due to the signal distortion.

In this paper, digital clipping is performed in the real domain, similarly for the in-phase and quadrature components. Taking the in-phase signal, I_k , as an example, the application of digital clipping can be described as

$$I_{k,clip} = \begin{cases} I_k / (1 - \frac{\kappa}{100}), & |I_k| < 1 - \frac{\kappa}{100} \\ \text{sgn}(I_k), & |I_k| \geq 1 - \frac{\kappa}{100} \end{cases} \quad (9)$$

where, once again, it is assumed that I_k is normalized in the range $[-1, 1]$, $I_{k,clip}$ represents the clipped signal, $\text{sgn}(\cdot)$ represents the sign function and $\kappa \in [0, 100]$ controls the amount of clipping (in percentage) to be applied to the I and Q components. Note that expression (9) already includes the re-normalization of the clipped signal to the range of $[-1, 1]$.

Clearly, the hard limitation on the maximum signal amplitude imposed by (9) gives rise to a compression effect of the modulated signal, which can be defined as

$$C_{clip} = -20 \log_{10} \left(1 - \frac{\kappa}{100} \right). \quad (10)$$

The impact of clipping strongly depends on the statistics of the transmitted digital signal, notably on its PAPR. For that reason, let us consider two extreme scenarios in order to bound the expected effect of clipping: i) the case of a QAM signal with an infinite number of symbols (∞ -QAM), so that the corresponding I_k and Q_k components are uniformly distributed, and ii) the case of a Gaussian-modulated signal, resembling the PCS trend, in which the I_k and Q_k components are exactly Gaussian distributed. Considering these two hypothetical scenarios, Fig. 3 shows the effects of amplification and compression (as per (10)) arising from the application of clipping according to (9). It is interesting to observe that, due to its higher PAPR, Gaussian modulation allows for higher power gains, thereby indicating that the optimization of digital clipping might play an important role

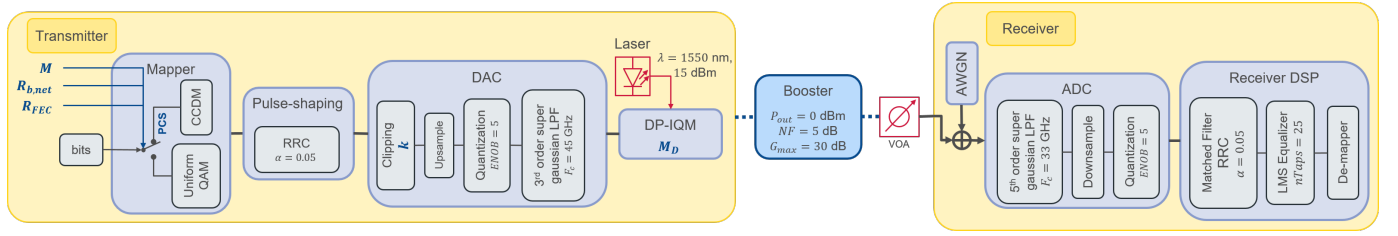


Fig. 4. Block diagram representing the key simulation steps and parameters.

in PCS signals. Note that a 6 dB increase in the transmitted power can be achieved by setting κ to 50%, which comes at the cost of a 6 dB compression of the signal. However, the impact of compression on a Gaussian or quasi-Gaussian signal is potentially less harmful than in an uniformly distributed signal, as fewer samples are affected by it. Whereas it is clear that digital clipping should be minor in scenarios without power constraints, in amplifier-less systems the extra launched power might compensate for the added distortion created by a more aggressive clipping. A comprehensive numerical analysis of this trade-off will be presented further ahead, in section III, considering different flavours of PCS modulation.

C. Forward Error Correction (FEC) rate and operation limits

In order to mitigate transmission errors, communication systems typically rely on algorithms to identify and correct any error that might occur. Forward error correction (FEC) algorithms are widely used for this purpose. However, we need to allocate a number of bits specifically for FEC at the transmitter that carry no information; this defines the FEC overhead, OH_{FEC} . Higher FEC overheads allow for the correction of more errors, but it leads to a decrease in the net bit rate, $R_{b,net}$.

The FEC overhead is the amount of added bits for a given payload. For instance, a value of $OH_{FEC} = 1/5$ means that, for each 5 bits of payload, 1 bit for FEC is added.

Throughout this work, we will refer to the FEC rate, R_{FEC} . The FEC rate is defined in terms of FEC overhead, OH_{FEC} , as

$$R_{FEC} = \frac{1}{OH_{FEC} + 1}. \quad (11)$$

For the previous example, this yields $R_{FEC} = 5/6$.

The concept of FEC rate is particularly important when we make use of probabilistic constellation shaping (PCS), since the probabilistic amplitude shaping (PAS) scheme defines limits for R_{FEC} that will be discussed below. Furthermore, the value of R_{FEC} defines the operation limit of the system in terms of normalized generalized mutual information (NGMI). The NGMI is given by [10]

$$NGMI(X; Y) = 1 - \frac{H(X) - GMI(X; Y)}{\log_2(M)}, \quad (12)$$

where X and Y represent the transmitted and received signal, respectively, $H(X)$ is the entropy of X , GMI is the generalized mutual information as given by [10, eq. (13)] and M is the number of symbols of the QAM template.

The minimum NGMI value required for error-free operation after FEC decoding is referred to as the NGMI threshold, $NGMI_{th}$. As we are assuming an ideal FEC decoder, the NGMI threshold is defined as $NGMI_{th} = R_{FEC}$ [10].

D. Probabilistic Constellation Shaping

Probabilistic constellation shaping (PCS) is a technique that can help achieve higher granularity in the bit rate [10]. In this work, we make use of probabilistic amplitude shaping (PAS), which shapes information bits with a Maxwell-Boltzmann (MB) distribution and the FEC parity bits are assigned based on the quadrant positions of the QAM signal [24]. The PAS rate, R_{PAS} , is defined as

$$R_{PAS} = \frac{R_{b,net}}{2R_s R_{FEC} \log_2(M_{PCS})}, \quad (13)$$

where $R_{b,net}$ defines the net bit rate, R_s defines the symbol rate, M_{PCS} defines the QAM template for the PCS, and R_{FEC} defines the FEC rate. The factor of 2 accounts for the two polarization tributaries. As shown, R_{PAS} is dependent on the FEC rate, and due to the implementation of the PAS scheme [25], we need to define limits of operation for R_{FEC} .

By definition, the PAS scheme imposes that a maximum of 2 bits per symbol (quadrant definition bits) are reserved for FEC overhead [24], which thereby restricts the minimum FEC rate to

$$R_{FEC} \geq 1 - \frac{2}{\log_2(M_{PCS})}. \quad (14)$$

Furthermore, the minimum R_{FEC} is also limited by the required net bit rate, defining another restriction,

$$R_{FEC} \geq \frac{R_{b,net}}{2R_s \log_2(M_{PCS})} + \frac{\log_2(M_{PCS}) - \log_2(M)}{\log_2(M_{PCS})}. \quad (15)$$

Note that the second right-hand side component of expression (15) accounts for the use of *non-regular* modulation orders, M , such as PCS-36QAM and PCS-100QAM, which actually rely on larger 2^n -QAM templates by setting to zero the probabilities of the outer symbols² [12].

As such, uniform constellations yield $R_{PAS} = 1$ for the case of 2^n -QAM constellations, but not for the case of *non-regular* QAM formats. The joint application of the aforementioned restrictions leads to the minimum R_{FEC} that can be implemented, $R_{FEC,min} = \max\{(14), (15)\}$. These boundaries for R_{FEC} will be considered to establish the simulation range in the following section.

²For instance, PCS-36QAM is actually built over a 64QAM template, and PCS-100QAM is built over a 256QAM template.

III. SIMULATION RESULTS

In this work, we start by simulating a coherent optical system. Our aim is to evaluate the performance of a short-reach amplifier-less coherent system. As such, our focus is to simulate a system without any amplification component. However, for a better understanding and completeness of this work, we will also compare the performance of this system to that of a system using transmitter-side optical amplification, henceforth referred to as *booster-aided* system.

A. Simulation Setup

A block diagram of the simulation setup can be seen in Fig. 4, where the use of a booster amplifier is optional, with the aim of providing a comparison with the amplifier-less system. The signal is defined with a symbol rate of 60 Gbaud and 2^{17} symbols. The transmitter laser operates with a power of 15 dBm. The digital-to-analog converter's (DAC) effective number of bits, ENOB, is set to achieve similar resolution as in the experiments, defining $\text{ENOB} = 5$ [26], and a factor of 4 is used in oversampling the *analog* waveform. In the transmitter, we define the QAM constellation order, M , the net bit rate, $R_{b,\text{net}}$, and the PAS rate, R_{PAS} (consequently setting the FEC rate, R_{FEC}). These variables will determine if the constellation is shaped or uniform. Constellation shaping is achieved through an ideal implementation of the constant composition distribution matching (CCDM), considering a block-size equal to the length of the transmitted/received signals, thereby rendering the impact of CCDM-induced rate loss negligible. As we aim to identify the fundamental impact of the amplifier-less assumption on shaped coherent optical systems without capturing implementation-specific penalties, the study of rate loss inherent to practical CCDM implementations is outside of the scope of this paper. A comprehensive study on the impact of coding and shaping gaps in practical PCS implementations can be found in [10]. We then apply a root-raised cosine (RRC) pulse shaper with roll-off factor, α , of 0.05 and with 2 samples per symbol. Another important variable in this study is the digital clipping applied to the transmitted signal, κ , which is applied before the digital-to-analog converter (DAC). After the DAC, the signal is sent to a dual-polarization (DP) in-phase and quadrature modulator (IQM), where we will define different values for the modulation depth (M_D). The signal is then attenuated with a variable optical attenuator (VOA) to emulate fiber transmission and to assess the power budget. We consider a close-to-ideal transmission by taking into account the signal attenuation and assuming ideal chromatic fiber dispersion compensation. At the receiver, additive white Gaussian noise (AWGN) with constant power is added to the attenuated signal ($P_{\text{noise}} = -38$ dBm at the symbol rate) in order to emulate the receiver sensitivity. The analog-to-digital converter (ADC) includes bandwidth restrictions to emulate experimental conditions, by applying a low-pass 5th order super-Gaussian filter with 33 GHz bandwidth, and a finite $\text{ENOB} = 5$. We then apply a matched filter (RRC with a roll-off factor of 0.05) and digital signal processing (DSP) techniques to mitigate impairments in the system, where we include a 2×2 least mean squares (LMS) equalizer.

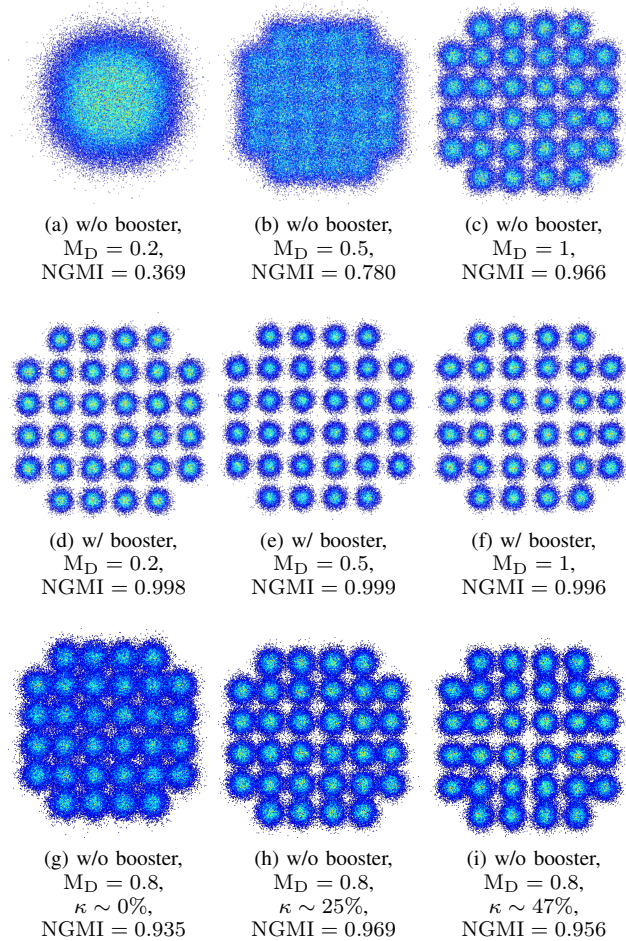


Fig. 5. Received constellations for a 32-QAM system with a net bit rate of 500 Gbit/s and with an attenuation of 15 dB, for different modulation depths (M_D).

Note that the inclusion of a dynamic equalizer allows the partial compensation of some non-ideal system parameters, such as limited ENOB and clipping, thus better mimicking a practical implementation scenario. After the demapper, the performance in terms of normalized generalized mutual information (NGMI) is analyzed.

In the setup with optical amplification, we define a constant output power of $P_{\text{out}} = 0$ dBm, unless the required gain exceeds the defined maximum gain of 30 dB for the optical booster, with a 5 dB noise figure. Note that in a field deployment, the booster gain should consider penalties induced by fiber nonlinearities due to high launch power. To take this into account, we have defined the booster to operate with a maximum output power of 0 dBm.

B. Performance Overview

In order to qualitatively analyze the impact of different modulation depths (M_D) and clipping percentages (κ), we can start by observing the respective distortions imposed on the received signal constellations. Figure 5 shows the received constellations for a uniform 32-QAM with a net bit rate $R_{b,\text{net}} = 500$ Gbit/s, for different values of M_D and κ . From

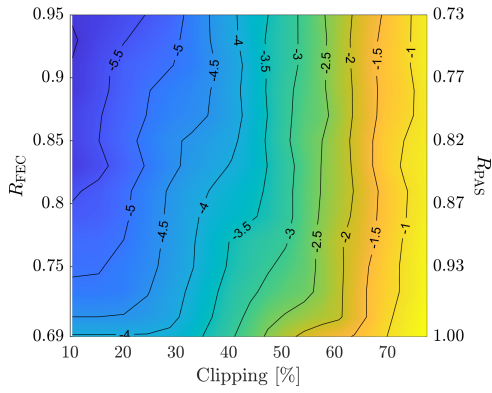


Fig. 6. Transmitted power for a 64-QAM system without booster operating at a net bit rate of 500 Gbit/s, for $M_D = 1$.

Fig. 5a to Fig. 5c, we can observe the impact of the modulation depth for an amplifier-less system without any clipping. For low values of M_D , the system noise is the major contributor to the poor performance. This shows that the system requires higher transmitted optical power, which can be achieved by increasing the IQM modulation depth. Indeed, the performance increases with M_D , being optimum for $M_D = 1$. From this figure, we can already conclude that there is a need to optimize the values of M_D to obtain the best performance. Figure 5 also shows the impact of the use of amplification (Fig. 5d to Fig. 5f): for low values of M_D , there is no evident penalty in performance. However, with $M_D = 1$ we can observe a slight loss in performance; this is because the system is reaching the nonlinear region. The improvement achieved by using optical amplification is evident, reaching higher values of NGMI. With this comparison, we can already see that the impact of the average power being sent to the system is of key importance.

Defining a fixed value for the modulation depth, $M_D = 0.8$, Fig. 5 also shows the impact of the clipping percentage applied at the transmitter for the amplifier-less case. We can immediately observe that there is a value of clipping that optimizes the performance of the system. In fact, low clipping percentages lead to low gains in performance. As the value for κ increases, we see an improvement in performance. However, high values of κ lead to poor performance, as expected, due to the introduced distortions. Overall, there is a tradeoff between the increased transmitted power enabled by digital clipping, and the signal distortions that are introduced in that process. The best system performance is achieved by optimizing the clipping percentage.

The focus of the remaining simulation is to optimize the aforementioned parameters, the modulation depth and clipping percentage, as well as the PAS rate, so that we can maximize the power budget, allowing for the deployment of short-reach amplifier-less systems.

C. Performance Analysis

In this section, we analyze the performance in terms of transmitted power and power budget for a set of system parameters. In this context, the transmitted power is evaluated

at the output of the emulated IQM and the power budget is defined as the maximum attenuation value that enables to operate above the theoretical NGMI threshold, NGMI_{th} (cf. section II-C: $\text{NGMI}_{\text{th}} = R_{\text{FEC}}$). We analyze the performance for different values of clipping percentage, κ , and different PAS rates, R_{PAS} , yielding different FEC rates (cf. (13)), for each modulation depth, M_D , modulation order, M , and net bit rate, $R_{\text{b,net}}$.

Figure 6 shows how the transmitted power is affected by both clipping, FEC and PAS rate. As expected, the transmitted power continuously increases with clipping, since we are forcing a lower PAPR. Furthermore, for low values of clipping, we observe the power penalty in applying shaping (lower R_{PAS} , higher R_{FEC}). However, due to the introduced distortion and rate optimization inherent to defining NGMI_{th} , the power gains shown will not be directly converted to power budget gains.

By sweeping the attenuation values for each pair of $\{\kappa, R_{\text{PAS}}\}$ (or, similarly, $\{\kappa, R_{\text{FEC}}\}$), we obtain a three-dimensional set of values for the NGMI. By assuming an ideal forward error correction (FEC) algorithm, we can easily define the NGMI threshold that allows for error-free decoding, i.e. $\text{NGMI}_{\text{th}} = R_{\text{FEC}}$. We can then obtain the attenuation that led to an NGMI of NGMI_{th} ; this is referred to as the power budget. We can now produce a heatmap showing the power budget for each $\{\kappa, R_{\text{PAS}}\}$ pair, for a set of parameters such as the modulation order, M , the modulation depth, M_D and the net bit rate, $R_{\text{b,net}}$. Figure 7 shows a few examples of these heatmaps, for the case of a 64-QAM 500 Gbit/s signal and for a set of modulation depths $M_D = \{0.2, 0.5, 1\}$. From Fig. 7a to Fig. 7c, the system includes a booster amplifier. In general, we observe that the power budget remains almost unchanged for a wide range of the considered parameters, evidencing a faint dependence of the booster-based system on the IQM modulation depth, signal clipping and shaping/coding. As a rule of thumb, both clipping and M_D can be safely kept at reasonably low values, while the optimization of shaping/coding only leads to about 0.5 dB variation in power budget. As expected, this shows that for systems with built-in optical amplification, the precise optimization of these parameters is not so critical. In contrast, for amplifier-less systems, depicted in Figs. 7d to 7f, we clearly observe that the optimization of these quantities is of utmost importance: the best performance is only achieved for high values of modulation depth ($M_D = 1$), high R_{PAS} values (i.e., quasi-uniform constellations with low shaping, meaning low R_{FEC}). Furthermore, the applied digital clipping should be optimized. While in Fig. 3 we observed increasing power with the clipping, here we observe a power penalty in applying too high clipping, highlighting the need to avoid the clipping-dominated region (above 60%).

By selecting the optimum $\{\kappa, R_{\text{PAS}}\}$ operating points (marked with a red cross in Figs. 7d to 7f), Fig. 8 shows the maximum achieved performance as a function of the modulation depth, M_D , considering different modulation format options that yield a net bit rate of 500 Gbit/s. Note that 32-QAM at 500 Gbit/s leads to a uniform constellation having $R_{\text{FEC}} = 5/6$. As expected for systems with optical

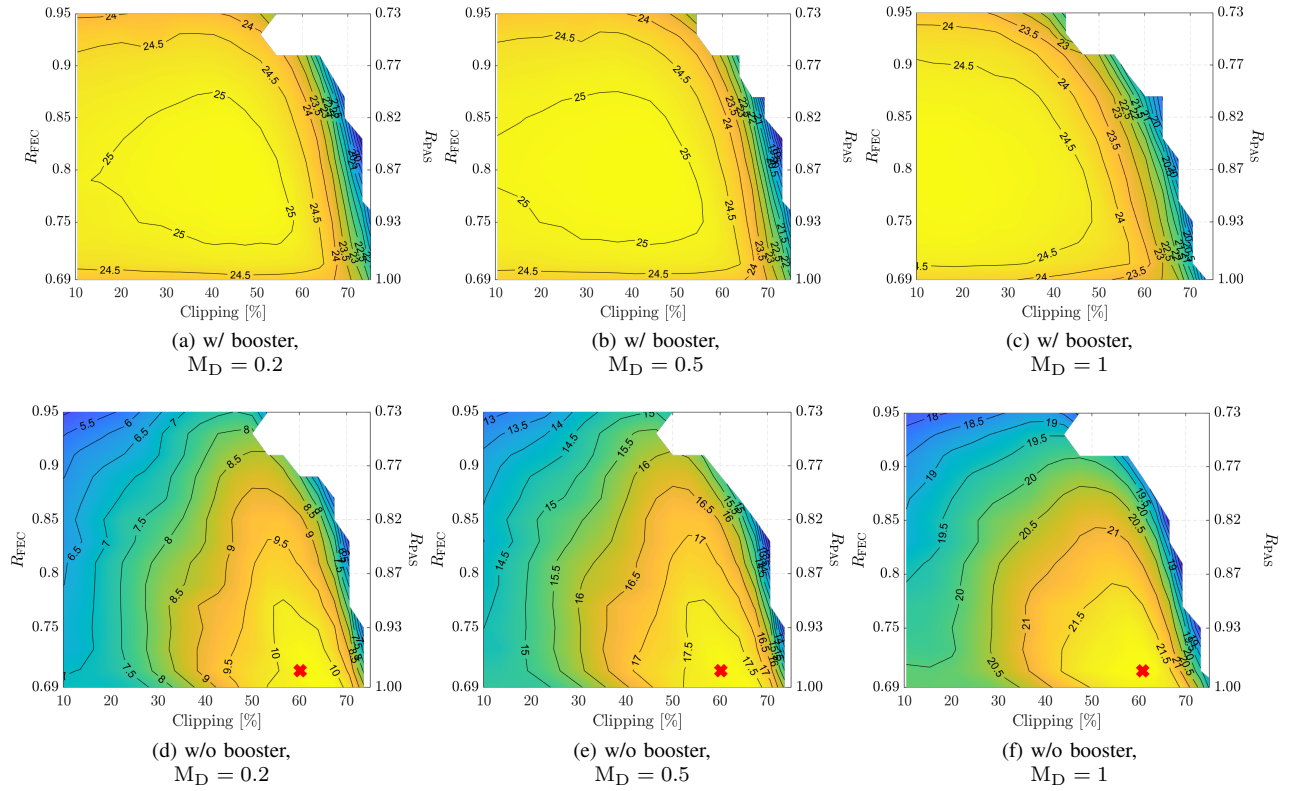


Fig. 7. Power budget for 64-QAM systems with a net bit rate of 500 Gbit/s, for variable modulation depths (M_D).

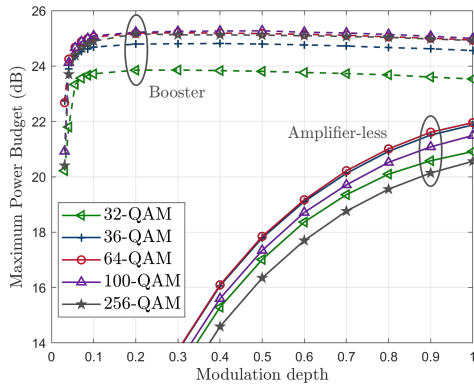


Fig. 8. Maximum power budget for each modulation depth (M_D), with a net bit rate $R_{b,net} = 500$ Gbit/s and different modulation formats.

amplification, the system performance tends to saturate with increasing constellation sizes, with 64-QAM, 100-QAM and 256-QAM presenting similar power budgets. Since the booster amplifier effectively compensates for the IQM insertion loss at low modulation depths, we can observe that the maximum power budget tends to flatten out for $M_D > 0.2$, then decreasing as it moves towards nonlinear compression at the IQM. Only for extremely low M_D we observe a steep loss of performance, which is mainly caused by the inability of the booster to compensate for IQM losses above 30 dB (maximum booster gain). In contrast, for the amplifier-less system whose results are also depicted in Fig. 8, we see that the power budget increases when increasing the modulation depth, but starts to

stabilize with higher values of M_D . This is because low values of M_D suffer from low launched power, while higher values start to increase the IQM nonlinearities. From these results, we can also conclude that 32-QAM is the format with the poorest performance, while 36-QAM and 64-QAM provide the highest power budget. It is also worth noting that, in contrast with the amplifier-aided system, both 100-QAM and 256-QAM solutions now yield approximately 0.5 dB and 1.4 dB performance penalty, respectively. This penalty is triggered by the increased PAPR of the higher-order constellations, which in conjunction with the lack of optical amplification, results in an effective reduction of the average transmitted optical power. Based on the results of Fig. 8, we now define the following optimized modulation depths for operation: $M_D = 0.2$ and $M_D = 1$ for a system with and without booster, respectively. The performance will now be further analyzed for these specific values.

Figure 8 does not show the optimization of both clipping and PAS rate. To show the importance of clipping, Fig. 9 shows the power budget achieved with each value of clipping, κ , for the optimum modulation depth (i.e., $M_D = 0.2$ for the system with booster and $M_D = 1$ for the amplifier-less case). As expected, we observe that using clipping does not lead to significant improvement in systems with optical amplification. In fact, even though the system can tolerate clipping values up to 40-50%, depending on the constellation size, the gain provided by clipping optimization is typically below 0.1 dB. As opposed to this behavior, amplifier-less results in Fig. 9 show major improvements in power budget by using clipping.

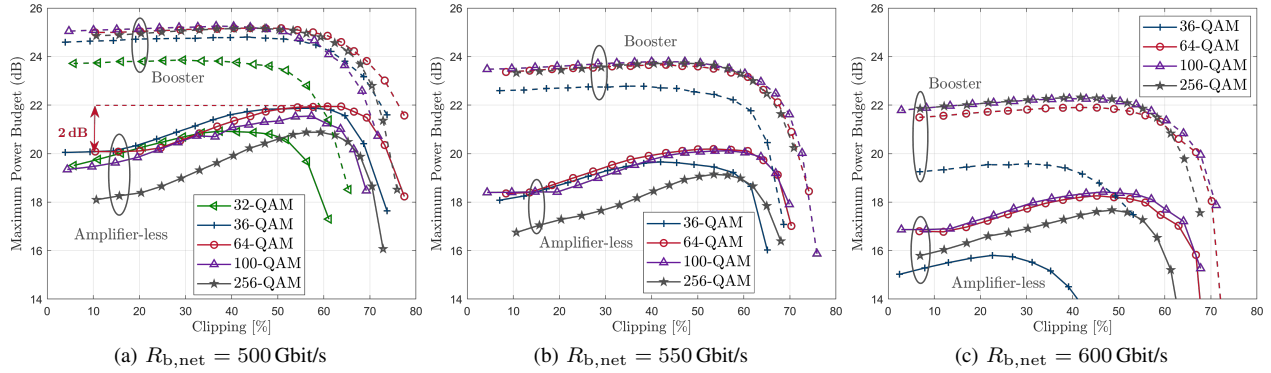


Fig. 9. Maximum power budget for each clipping percentage, κ , for the amplifier-less and booster systems at 500 Gbit/s, 550 Gbit/s and 600 Gbit/s.

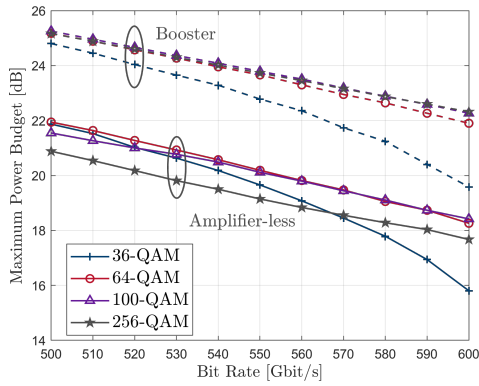


Fig. 10. Maximum power budget for each net bit rate, $R_{b,net}$, for the amplifier-less and booster systems.

For each modulation order, the behavior is similar: the power budget tends to steadily increase with stronger clipping, up to a point where the optimum κ value is found. Afterwards, the strong distortion imposed upon the clipped signal rapidly degrades the performance. In contrast with the booster-aided scenario, in which the gain provided by clipping was found to be almost negligible, we can now observe sizeable gains of approximately 2 dB for the amplifier-less system, solely enabled by digital clipping optimization. Furthermore, we observe no gain in using higher modulation formats (100-QAM and 256-QAM), with a power budget saturation being achieved in the booster-aided system and power penalty being observed for the case of amplifier-less system. Figure 9 also reveals that, despite the different relative performances, the same overall trend is followed for different bit rates.

Following the same optimization steps described so far, Fig. 10 shows the maximum power budget obtained for different net bit rates, from 500 Gbit/s up to 600 Gbit/s, with steps of 10 Gbit/s. For each $R_{b,net}$, we present the maximum power budget that corresponds to an optimized pair of parameters $\{\kappa, R_{PAS}\}$. The value for M_D is kept constant at $M_D = 1$ for the amplifier-less case and $M_D = 0.2$ for the system with booster. While for the booster-aided system we can verify that the optimum performance can always be achieved by using large QAM constellations, it is interesting to observe how the adaptation of net bit rate interplays with the

optimum choice of modulation format for the amplifier-less system. On one hand, using excessively large constellations yields a penalty in power budget, caused by the PAPR-inflicted loss of transmitter power. To further exacerbate this effect, we have added a 256-QAM curve to Fig. 10, which clearly reveals the performance penalty associated with an over-dimensioning of the PCS constellation. However, on the other hand, restricting the constellation size to the lowest supported QAM order might also be suboptimal, as it imposes the use of very high R_{FEC} (i.e. low FEC overhead), as pointed out in recent works exploring the tradeoff between coding and shaping in AWGN systems [10], [27], we observe that extreme conditions in which the coding rate tends to unity are in general suboptimal. However, the impact of modulation depth and clipping-induced nonlinear distortions requires a comprehensive re-optimization of the R_{FEC}/R_{PAS} tradeoff. This tradeoff is clearly visible as we move from 500 Gbit/s to 600 Gbit/s in Fig. 10: while 36-QAM provides a near-optimum solution at 500 Gbit/s, it becomes largely suboptimal at 600 Gbit/s. It is also interesting to note that while 64-QAM yields the highest power budget for bit rates up to 560 Gbit/s, 100-QAM then becomes the preferred solution at larger bit rates. In general, this analysis demonstrates that the choice of modulation format in amplifier-less systems is non-trivial, as it requires the multi-dimensional optimization of several key parameters at play.

Figure 11 shows the optimized parameters that provide the power budget values in Fig. 10, where the marks represent the collected simulated data and the dotted lines represent a linear regression of these points. Note that R_{FEC} and R_{PAS} are tied to the same net bit rate, following expression (13). In general, the optimum performance in amplifier-less systems tends to be primarily dictated by the optimization of the PCS rate, i.e. the amount of shaping that is applied to the constellation. These results can be seen in Fig. 11a, where the maximum power budget solutions (64-QAM for $R_{b,net} \in [500, 550]$ Gbit/s and 100-QAM $R_{b,net} \in [560, 600]$ Gbit/s) are obtained for quasi-uniform constellations. As previously concluded, the amount of constellation shaping in amplifier-less systems must be kept low, in order to avoid the detrimental impact of high PAPR on the achievable transmitted power. The corresponding FEC rates are displayed in Fig. 11b. Here, it can also be concluded

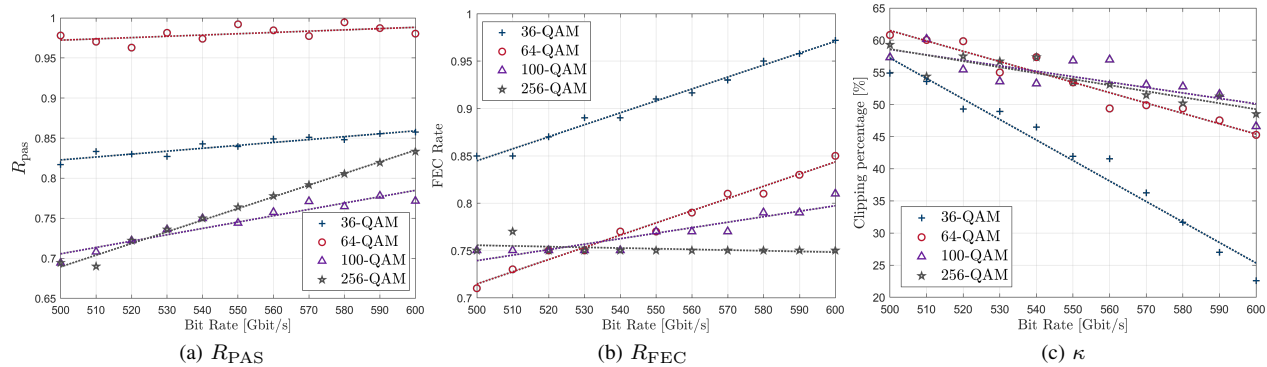


Fig. 11. Optimum parameters chosen for each optimum point at a given net bit rate, $R_{b,net}$, for the amplifier-less system.

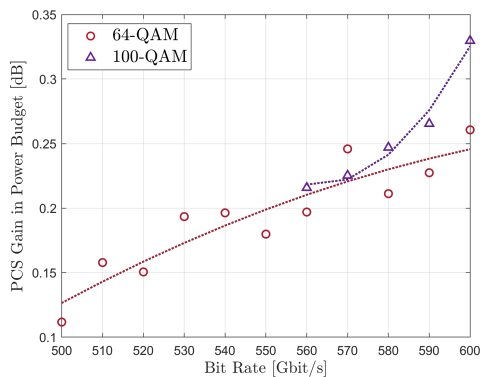


Fig. 12. PCS power budget gain when compared to using uniform constellations, for each bit rate, for the system without booster, for each modulation order.

that the maximum power budget solution should, in general, keep a low enough FEC rate (typically below 0.85), i.e. a large FEC overhead. Note that FEC optimization should still be performed to avoid the introduction of power penalties inherent to fixed FEC rate solutions. In fact, [27] shows that both too-low and too-high FEC rates introduce power penalties that become more evident with higher modulation order. Finally, the optimized digital clipping values are shown in Fig. 11c. As expected, the optimized clipping follows the inverse trend of the R_{PAS} values, i.e. higher clipping is required for more strongly shaped constellations, while less clipping must be used for quasi-uniform constellations. It is also interesting to note that all these quantities seem to quasi-linearly depend on the transmitted net bit rate, a property that might be used to establish simplified operation rules for amplifier-less optical systems with bit rate adaptation.

The obtained results so far have shown that the optimum solutions for amplifier-less systems are generally based on quasi-uniform constellations. However, it is still not clear whether there is a sizeable benefit of applying any constellation shaping at all in these systems. In order to shine some light over this issue, in Fig. 12 we show the PCS-enabled increase in power budget, which is obtained by comparing each modulation order to its correspondent uniform constellation (i.e., maximum supported R_{PAS}), optimizing the clipping for both PCS and uniform constellations. For

simplicity of representation, we show only the two best modulation options that have been identified for the range of bit rates under test: 64-QAM and 100-QAM. While the gain provided by PCS is indeed far from what can be achieved in booster-aided systems, we still observe a residual gain in the range of 0.1–0.3 dB in power budget. (Note that for the case of 64-QAM at 500 Gbit/s, this gain can be observed in Fig. 7f.) It is also interesting to note that the PCS gain in these systems tends to increase with the transmitted bit rate (for a fixed symbol rate), which shows that, while less significant, the use of PCS can also be advantageous for amplifier-less systems. This analysis assumes an ideal implementation of the distribution matcher (DM). However, realistic DMs introduce penalties that depend on the implementation. A poorly chosen implementation can overthrow the small gains that are being shown; as such, the DM implementation should be carefully chosen to have a minimum rate loss, yielding to a lower penalty. A detailed study on the rate loss can be found in [10].

IV. EXPERIMENTAL SETUP

In order to verify the main conclusions obtained from the previously discussed simulation results, in this section we proceed with an experimental validation campaign in similar operating conditions. Figure 13 shows a block diagram of the experimental setup. The transmitter is composed of an external cavity laser (ECL) operating at $\lambda = 1550$ nm, with a power of 14.5 dBm. The 60 Gbaud signal is generated by the transmitter (Tx) digital signal processing (DSP) block, sending samples to the arbitrary waveform generator (AWG) with 45 GHz bandwidth and operating at 120 Gsamples/s. The signal is then sent to a dual-polarization in-phase and quadrature modulator (DP-IQM) with a bandwidth of approximately 45 GHz. After the transmitter, a variable optical attenuator (VOA) enables the power budget study. The signal is forwarded to the polarization-diverse coherent receiver with a bandwidth of ~ 40 GHz. The local oscillator (LO) is an ECL operating at $\lambda = 1550$ nm and a power of 13 dBm. A four-port oscilloscope with 33 GHz of bandwidth digitizes the signal at 100 Gsample/s before the receiver (Rx) DSP. Here, we apply a Gram-Schmidt orthonormalization algorithm, a constant modulus algorithm (CMA) supporting radius-directed

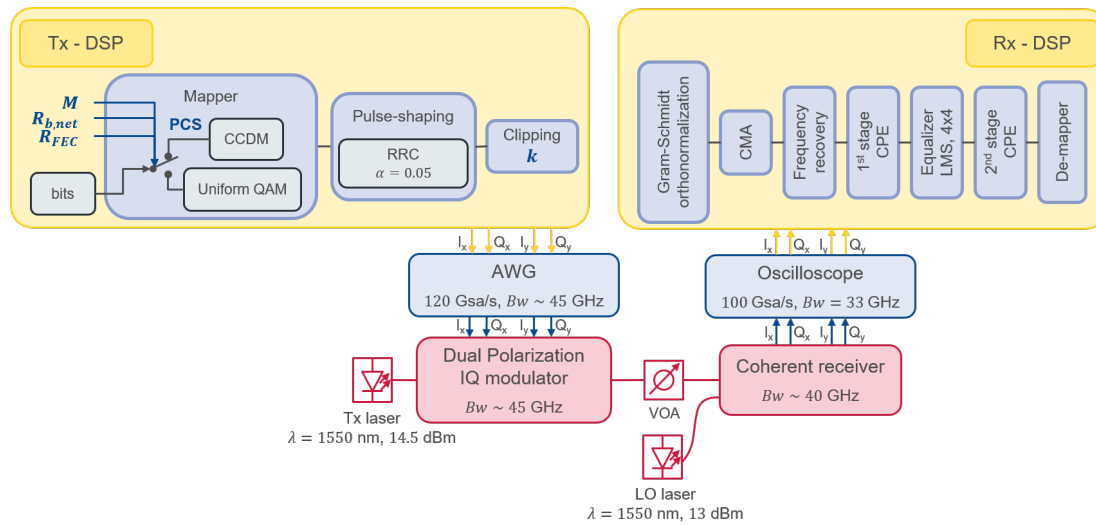
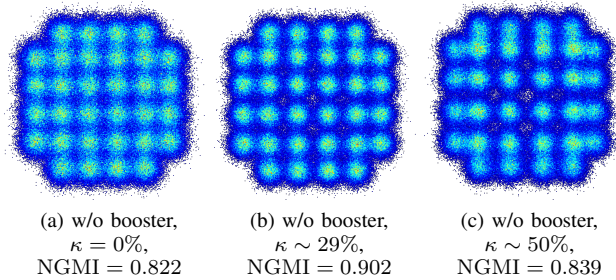
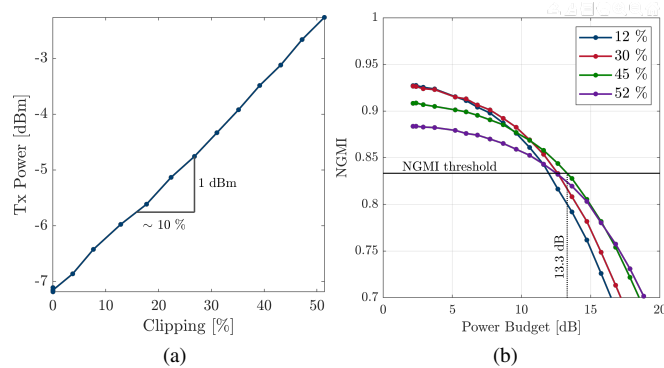


Fig. 13. Block diagram of the experimental amplifier-less setup

Fig. 14. Experimentally received constellations for a 32-QAM signal with a net bit rate of 500 Gbit/s, with an attenuation of 14.7 dB and $R_{FEC} = 5/6$, for different clipping percentages (κ).Fig. 15. Performance dependency on the applied digital clipping for the case of 64QAM at 600 Gbit/s with $R_{FEC} = 5/6$. a) Tx power dependency on the clipping; b) NGMI vs power budget for different clipping percentages.

equalization [28], frequency recovery and a first stage of pilot-based carrier phase estimation (CPE) [29], followed by a least-mean squares (LMS) equalizer and a final stage of CPE. The applied algorithms are genie aided to emulate an ideal DSP, allowing us to discard impairments that would draw focus from the impact of the key parameters that are central for this study. Note that, for practical implementation reasons, in

the following experimental analysis we have kept the AWG output voltages fixed, and thus the IQ modulation depth is also fixed. The reasons for this implementation choice are two-fold: i) fixing the AWG output voltage significantly simplifies the experimental setup conditions, as it avoids the need for a time-consuming additional sweep of the IQ modulation depth and ii) due to the additional compression points of the IQ modulator drivers, it would be hard to identify the exact sources of distortion. Therefore, we have performed a set of preliminary tests leading to an optimized AWG voltage providing a conservative optimum point of operation (i.e., avoiding a high compression region), for a given set of signal parameters, and then the AWG voltages were maintained throughout the work. The optimization of the launched optical power will then be controlled through the application of clipping over the digital signal. From a practical implementation standpoint, this also represents a major advantage, as it avoids the need to act over the analog frontend of the coherent transceiver, keeping all optimization variables in the digital domain.

A. Experimental Results

Figure 14 shows experimentally received constellations for a 32-QAM signal at 500 Gbit/s and with a FEC rate of $R_{FEC} = 5/6$. In this figure, we can observe the impact of clipping on the constellation and on the NGMI: in Fig. 14a we see the results with no clipping applied, Fig. 14b shows the optimum applied clipping, $\kappa \sim 29\%$, resulting on the best NGMI and Fig. 14c shows the worst NGMI when too much clipping is applied. From these results, we reiterate the key role of digital clipping played in amplifier-less coherent systems, showing that even a high clipping percentage is preferred to no clipping. With these constellations, we observe that increasing the clipping has a similar effect as increasing the modulation depth on the DP-IQM, with clear advantages in terms of flexibility and power consumption.

The impact of clipping can also be seen in Fig. 15 for the case of 64QAM at 600 Gbit/s with $R_{FEC} = 5/6$. First,

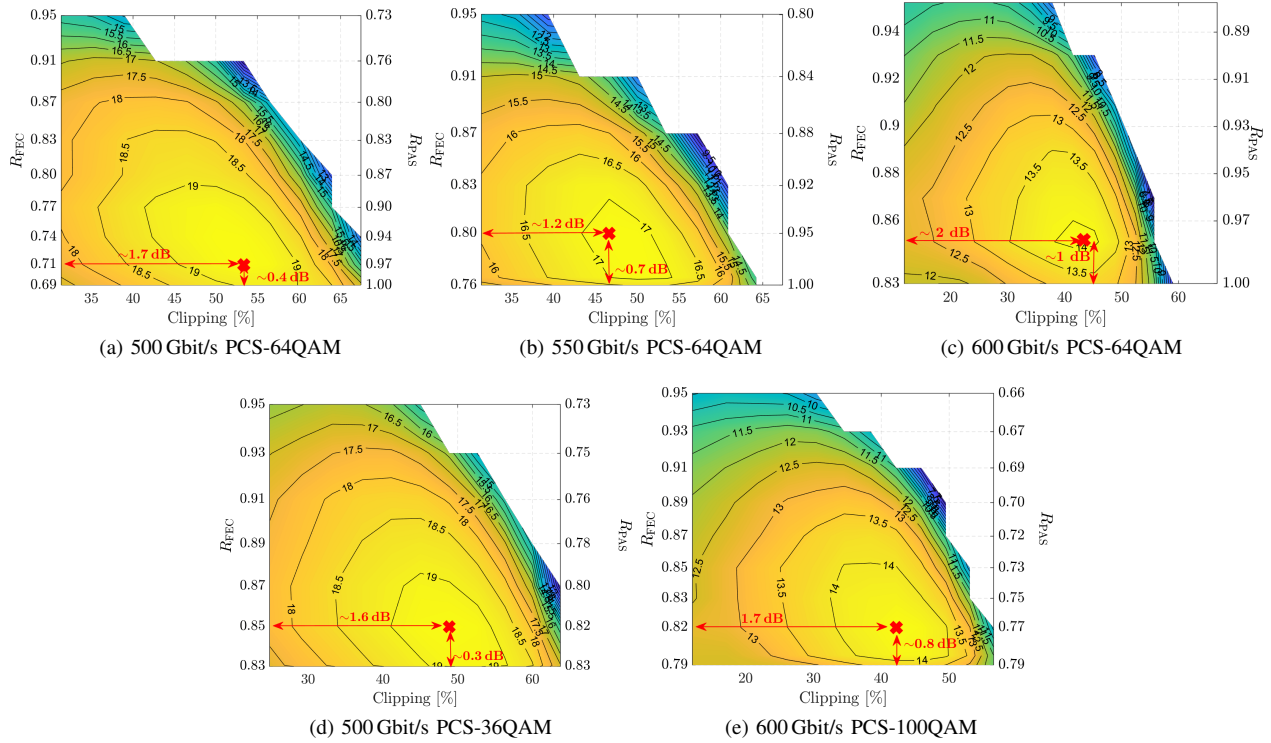


Fig. 16. Experimentally measured power budget at the NGMI threshold as a function of FEC rate, R_{FEC} , and clipping percentage, κ

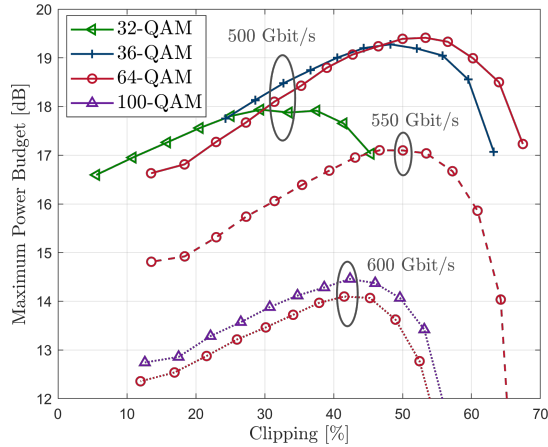


Fig. 17. Impact of digital clipping on the maximum power budget with pre-optimized R_{PAS}/R_{FEC} optimization at different net bit rates.

Fig. 15a shows a linear dependency of the transmitted power, measured at the output of the IQM, on the applied digital clipping. From this figure, we observe that, on average, each 10 % of clipping leads to a 1 dB increase in transmitted power. By comparing these results to the theoretical analysis in Fig. 3a, we observe that this power gain is within the bounds of the ∞ -QAM and the Gaussian modulated signals. Figure 15b shows how the NGMI evolves with the applied attenuation, for different values of clipping. We see that $\kappa \sim 45\%$ is the clipping value that leads to the highest power budget of 13.3 dB.

Figure 16 shows the bi-dimensional optimization of the power budget of the parameter pair $\{R_{FEC}, \kappa\}$ (or $\{R_{PAS}, \kappa\}$),

TABLE I
SUMMARY OF BEST EXPERIMENTAL PERFORMANCES AND OPTIMIZED PARAMETERS.

	$R_{b,net}$ [Gbit/s]	Power budget [dB]	R_{FEC}	R_{PAS}	κ [%]	M
PCS	500	19.3 ³	0.85	0.82 ⁴	48.2	36
	550	17.1	0.80	0.95	46.7	64
	600	14.5	0.82	0.77 ⁵	42.4	100
Uniform	500	17.9	5/6	N/A	37.5	32
	550	16.5	0.76	1	50.1	64
	600	13.3	5/6	1	41.5	64

for different modulation orders and net bit rates. With these results, we observe that the optimum value of clipping percentage decreases with the PAS rate, R_{PAS} , and with the increase of R_{FEC} , which was equivalently observed in terms of PAPR and coding overhead in [22]. We experimentally confirm that the use of clipping introduces a gain in power budget up to ~ 2 dB for the case of PCS-64QAM at 600 Gbit/s (see Fig. 16c), using similar R_{FEC} values. We also observe that the optimum power budget is ~ 1 dB higher when compared with the corresponding clipping percentage at $R_{PAS} = 1$; i.e., PCS is introducing a small but non-negligible gain. Nevertheless, these results confirm that the use of minor shaping introduces gain, and that R_{PAS} should also be optimized as higher shaping (lower R_{PAS} , higher R_{FEC}) leads to a decrease in performance.

³PCS-64QAM achieves a similar power budget. However, because it requires a higher FEC overhead ($OH_{FEC} \sim 30\%$ or $R_{FEC} = 0.77$), PCS-36QAM becomes the most feasible solution.

⁴36-QAM at 500 Gbit/s yields a uniform distribution for $R_{PAS} = 0.83$

⁵100-QAM at 600 Gbit/s yields a uniform distribution for $R_{PAS} = 0.79$

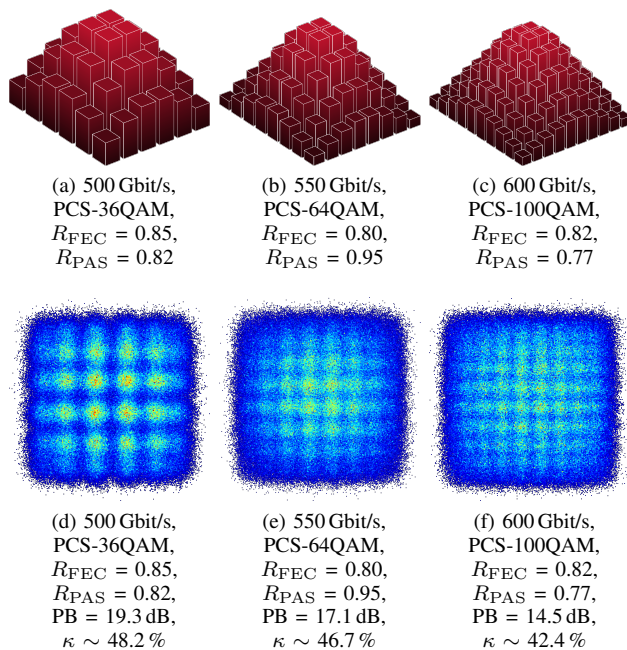


Fig. 18. Distribution of the symbol probability for the optimized constellations. PB: Power budget.

In Fig. 17 we show the evolution of power budget with the applied digital clipping, after pre-optimization of the optimum $R_{\text{FEC}}/R_{\text{PAS}}$ values (note that the 32-QAM solution is only uniformly distributed). We confirm the trend shown in the amplifier-less simulation setup of Fig. 9, as the power budget slowly increases, reaching the optimum clipping, after which there is a rapid decrease. Finally, the overall optimization of power budget and $R_{\text{FEC}}/R_{\text{PAS}}/\kappa$ parameters for different net bit rates is shown in Table I. Focusing on the practical implementation aspect, we have limited the FEC overhead to a maximum of 30% ($R_{\text{FEC}} \sim 0.77$), thus avoiding the use of power-hungry FEC solutions. As previously concluded from the simulation results, it can be seen that the best performances tend to be obtained with quasi-uniform constellations, together with FEC rates in the range of 0.8–0.85, corresponding to moderate overheads of ~ 17 –25%. The corresponding optimized PCS distributions and received signal constellations are depicted in Fig. 18. While the well-known shaping gain is indeed severely attenuated in amplifier-less scenarios, it is interesting to note that the use of PCS modulation plays an important role in simplifying the use of intermediate square QAM constellations with non-integer number of bits per symbol, as it is the case of 36QAM and 100QAM, which have provided the best performance at 500 Gbit/s and 600 Gbit/s, respectively. In order to highlight this fact, in the bottom part of Table I, we show the best power budgets and optimized parameters obtained with uniform 2^n -QAM constellations conveying n bits per symbol, such that the PCS technology can be avoided. For a fair comparison, we also consider a maximum FEC overhead of 30% for the uniform QAM solutions. Under this condition, we observe significant gains of the PCS solutions enabled by the use of QAM templates of optimized size.

V. CONCLUSION

In short-reach applications, contrary to long-haul coherent optical transmission systems, the well-known shaping gain provided by PCS is put at challenge due to the transmitter-side power constraint, caused by the lack of optical amplification. Targeting the emerging use case of amplifier-less coherent systems, in this work we have shown that the use of PCS can still be beneficial, provided that it is carefully optimized. It is also shown that the optimization of digital clipping and IQ modulation depth play a key role in amplifier-less coherent transceivers, as they enable to reduce the impact of modulation-induced loss, thereby increasing the effective transmitted optical power. Both simulation and experimental results support this claim, presenting an increase in power budget of 2 dB when compared to not applying clipping. Our simulation and experimental results have shown that optimized PCS constellations in amplifier-less systems tend to converge to a quasi-uniform symbol distribution, therefore yielding a lower shaping gain. For example, for a 64-QAM system at 550 Gbit/s, we have experimentally observed an increase in power budget of 0.6 dB when we compare the use of PCS and uniform constellation. Nevertheless, the use of PCS modulation still provides important additional degrees of freedom for the optimization of performance, namely by enabling the use of square QAM templates with non-integer number of bits per symbol, which provide a better fit to the required bit rate and operating baud rate. In such conditions, power budget gains exceeding 1 dB can still be enabled by PCS (experimentally achieving 1.2 dB at 600 Gbit/s between 100-QAM and uniform 64-QAM), while keeping a reasonably low FEC overhead. As a consequence, high order modulation formats, such as 100-QAM and 256-QAM, suffer from increased penalty due to the inherently higher PAPR.

Because digital clipping plays such an important role in the optimization of an amplifier-less system, further focus on the optimization of the constellation can lead to higher gains when compared to uniform 2^n -QAM. In fact, the Maxwell-Boltzmann (MB) probability distribution inherent to the employed PCS is found to be suboptimal for the system in analysis in this work. When the MB distribution constraint is lifted, the optimization of the input symbol probabilities can be performed resorting to adequate numerical approaches [9], [30]. Furthermore, because clipping affects the position of the outer symbols in the constellation, it can be viewed as a limited form of geometric shaping. Nevertheless, further geometric shaping optimization [31] could be performed to increase the observed gain when compared to uniform 2^n -QAM.

REFERENCES

- [1] P. J. Winzer, D. T. Neilson, and A. R. Chraplyvy, "Fiber-optic transmission and networking: the previous 20 and the next 20 years [invited]," *Opt. Express*, vol. 26, no. 18, pp. 24 190–24 239, 2018.
- [2] C. Xie and J. Cheng, "Coherent optics for data center networks," in *2020 IEEE Photonics Society Summer Topicals Meeting Series (SUM)*, 2020.
- [3] OIF, "Implementation agreement 400ZR," 2020.
- [4] A. Shahpari, R. M. Ferreira, R. S. Luis, Z. Vujicic, F. P. Guiomar, J. D. Reis, and A. L. Teixeira, "Coherent access: A review," *Journal of Lightwave Technology*, vol. 35, no. 4, pp. 1050–1058, 2017.

- [5] J. K. Perin, A. Shastri, and J. M. Kahn, "Design of low-power DSP-free coherent receivers for data center links," *Journal of Lightwave Technology*, vol. 35, no. 21, pp. 4650–4662, 2017.
- [6] K. Nishimura, S. Ishimura, A. Bekkali, K. Tanaka, H. Hirayama, Y. Tsukamoto, S. Nanba, and M. Suzuki, "Optical access technology for B5G MFH/MBH," in *Optical Fiber Communication Conference (OFC) 2019*, 2019, paper W3J.1.
- [7] B. Schrenk, D. Milovančev, N. Vokić, and F. Karinou, "Coherent homodyne TDMA receiver based on TO-can EML for 10 Gb/s OOK with <40 ns guard interval," in *Optical Fiber Communication Conference (OFC) 2020*, 2020, paper W4G.4.
- [8] M. Schmitt, "Coherent technologies and requirements in next-generation MSO networks," in *Optical Fiber Communication Conference (OFC) 2020*, 2020, paper Th1D.6.
- [9] A. Fallahpour, F. Alishahi, A. Minoofar, K. Zou, A. Almaini, P. Liao, H. Zhou, M. Tur, and A. E. Willner, "16-QAM probabilistic constellation shaping by learning the distribution of transmitted symbols from the training sequence," in *Optical Fiber Communication Conference (OFC) 2020*, 2020, paper M1G.3.
- [10] J. Cho and P. J. Winzer, "Probabilistic constellation shaping for optical fiber communications," *Journal of Lightwave Technology*, vol. 37, no. 6, pp. 1590–1607, 2019.
- [11] A. Mirani, M. Mazur, E. Agrell, B. Foo, J. Schröder, P. Andrekson, and M. Karlsson, "Comparison of uniform cross QAM and probabilistically shaped QAM formats under the impact of transmitter impairments," in *45th European Conference on Optical Communication (ECOC 2019)*, 2019, paper Th.2.B.3.
- [12] F. Buchali, W. Idler, R. Dischler, T. Eriksson, and L. Schmalen, "Spectrally efficient probabilistically shaped square 64 QAM to 256 QAM," in *2017 European Conference on Optical Communication (ECOC)*, 2017, paper Tu.2.D.1.
- [13] P. Dong, A. Melikyan, K. Kim, N. Kaneda, B. Stern, and Y. Baeyens, "In-phase/quadrature modulation by directly reflectivity modulated laser," in *Optical Fiber Communication Conference (OFC) 2020*, 2020, paper M2B.2.
- [14] A. Mecozzi, C. Antonelli, and M. Shtaif, "Kramers–Kronig coherent receiver," *Optica*, vol. 3, no. 11, p. 1220, 2016.
- [15] A. Lorences-Riesgo, F. P. Guiomar, A. N. Sousa, A. L. Teixeira, N. J. Muga, and P. P. Monteiro, "200 Gbit/s free-space optics transmission using a Kramers-Kronig receiver," in *Optical Fiber Communication Conference (OFC) 2019*, 2019, paper W4A.3.
- [16] P. Dong, X. Chen, K. Kim, S. Chandrasekhar, Y.-K. Chen, and J. H. Sinsky, "128-Gb/s 100-km transmission with direct detection using silicon photonic stokes vector receiver and I/Q modulator," *Optics Express*, vol. 24, no. 13, p. 14208, 2016.
- [17] Y.-W. Chen, R. Zhang, S.-J. Su, S. Shen, Q. Zhou, S. Yao, and G.-K. Chang, "Asynchronous multi-service fiber-wireless integrated network using UPMC and PS for flexible 5G applications," in *Optical Fiber Communication Conference (OFC) 2020*, 2020, paper M2H.4.
- [18] F. P. Guiomar, A. Lorences-Riesgo, D. Ranzal, F. Rocco, A. N. Sousa, M. A. Fernandes, B. T. Brandao, A. Carena, A. Teixeira, M. C. R. Medeiros, and P. P. Monteiro, "Adaptive probabilistic shaped modulation for high-capacity free-space optical links," *Journal of Lightwave Technology*, pp. 1–1, 2020.
- [19] P. Zou, F. Hu, G. Li, and N. Chi, "Optimized QAM order with probabilistic shaping for the nonlinear underwater VLC channel," in *Optical Fiber Communication Conference (OFC) 2020*, 2020, paper Th1K.7.
- [20] H. Sun, M. Torbatian, M. Karimi, R. Maher, S. Thomson, M. Tehrani, Y. Gao, A. Kumpera, G. Soliman, A. Kakkar, M. Osman, Z. A. El-Sahn, C. Doggart, W. Hou, S. Sutarwala, Y. Wu, M. R. Chitgarha, V. Lal, H.-S. Tsai, S. Corzine, J. Zhang, J. Osenbach, S. Buggaveeti, Z. Morbi, M. I. Olmedo, I. Leung, X. Xu, P. Samra, V. Dominic, S. Sanders, M. Ziari, A. Napoli, B. Spinnler, K.-T. Wu, and P. Kandappan, "800G DSP ASIC design using probabilistic shaping and digital sub-carrier multiplexing," *Journal of Lightwave Technology*, vol. 38, no. 17, pp. 4744–4756, 2020.
- [21] Y. Loussouarn and E. Pincemin, "Probabilistic-shaping DP-16QAM CFP-DCO transceiver for 200G upgrade of legacy metro/regional WDM infrastructure," in *Optical Fiber Communication Conference (OFC) 2020*, 2020, paper M2D.2.
- [22] A. Lorences-Riesgo, F. P. Guiomar, B. M. Oliveira, M. C. R. Medeiros, and P. P. Monteiro, "Joint optimization of coding, shaping and clipping for amplifier-less coherent optical systems," in *Optical Fiber Communication Conference (OFC) 2020*, 2020, paper Th1G.1.
- [23] J. C. M. Diniz, F. D. Ros, E. P. da Silva, R. T. Jones, and D. Zibar, "Optimization of DP-M-QAM transmitter using cooperative coevolutionary genetic algorithm," *Journal of Lightwave Technology*, vol. 36, no. 12, pp. 2450–2462, 2018.
- [24] G. Bocherer, P. Schulte, and F. Steiner, "Probabilistic shaping and forward error correction for fiber-optic communication systems," *Journal of Lightwave Technology*, vol. 37, no. 2, pp. 230–244, 2019.
- [25] G. Bocherer, F. Steiner, and P. Schulte, "Bandwidth efficient and rate-matched low-density parity-check coded modulation," *IEEE Transactions on Communications*, vol. 63, no. 12, pp. 4651–4665, 2015.
- [26] R. A. Belcher, "ADC standard IEC 60748-4-3: Precision measurement of alternative ENOB without a sine wave," *IEEE Transactions on Instrumentation and Measurement*, vol. 64, no. 12, pp. 3183–3200, 2015.
- [27] J. Cho, "Balancing probabilistic shaping and forward error correction for optimal system performance," in *Optical Fiber Communication Conference*. Optical Society of America, 2018, paper M3C.2.
- [28] M. Magarini, L. Barletta, A. Spalvieri, F. Vacondio, T. Pfau, M. Pepe, M. Bertolini, and G. Gavioli, "Pilot-symbols-aided carrier-phase recovery for 100-G PM-QPSK digital coherent receivers," *IEEE Photonics Technology Letters*, vol. 24, no. 9, pp. 739–741, may1, 2012.
- [29] I. Fatadin, D. Ives, and S. J. Savory, "Blind equalization and carrier phase recovery in a 16-qam optical coherent system," *Journal of Lightwave Technology*, vol. 27, no. 15, pp. 3042–3049, 2009.
- [30] J. Renner, T. Fehenberger, M. P. Yankov, F. D. Ros, S. Forchhammer, G. Böcherer, and N. Hanik, "Experimental comparison of probabilistic shaping methods for unrepeated fiber transmission," *J. Lightwave Technol.*, vol. 35, no. 22, pp. 4871–4879, Nov 2017.
- [31] B. Chen, C. Okonkwo, H. Hafermann, and A. Alvarado, "Increasing achievable information rates via geometric shaping," in *2018 European Conference on Optical Communication (ECOC)*, 2018, pp. 1–3.